

Modeling and analysis of a low-actuation-voltage MEM mirror with spring structure for tunable optical filter

Mohammad A. Matin

Yun-Bo Yi

Vikram Gogte

University of Denver

School of Engineering and Computer Science

2390 S. York Street

Denver, Colorado 80208

E-mail: mmatin@du.edu

Abstract. Tunable optical filters are key components for dense wavelength-division-multiplexed (DWDM) optical networks. One of the successful mechanisms to realize the wavelength tunability is by utilizing micro-electromechanical systems (MEMS) technology. The tuning mechanism works by applying a voltage between the top mirror and the bottom electrode. Micromechanically actuated optical filters are desirable because of their wide tuning range and process compatibility with other optoelectronic devices. Modeling and simulation play important roles in the MEMS domain. In this paper, we present four different mirror models. A detailed theoretical analysis including both static and dynamic aspects was developed on the four mirror models. A record tuning range of 149 nm with a very small actuation voltage of 2.5 V is achieved for the MEMS-based tunable optical filter. © 2007 Society of Photo-Optical Instrumentation Engineers. [DOI: 10.1117/1.2731364]

Subject terms: Optical filter; micro-electro-mechanical systems; micromirror.

Paper 06062RR received Aug. 30, 2006; revised manuscript received Dec. 14, 2006; accepted for publication Dec. 20, 2006; published online Apr. 18, 2007.

1 Introduction

An optical filter is a component or device that selectively transmits or reflexes a range of wavelengths.¹ With the advent of dense wavelength-division multiplexing, tunable devices have gained significant importance due to a considerable reduction in inventory costs. Recently, there has been an increasing need for inexpensive and flexible components such as tunable lasers, tunable filters, and tunable detectors in all-optical network systems and sensor applications. Many promising approaches have been studied, including Fabry–Perot, acousto-optic, electro-optic, and liquid-crystal Fabry–Perot filters.^{2–4} Tunable optical filters (TOFs) are key components, with advantages of low insertion loss, small size, and large tuning range for reconfiguring the flexible networks.¹ Fabry–Perot interferometers,² Fiber–Bragg gratings,³ electro-optics,⁴ and acousto-optics⁵ are some of techniques with which TOFs can be implemented. In this research, the Fabry–Perot optical filtering approach is taken into consideration.

The tunable optical filter is efficient in selectively adding or dropping particular wavelength channels from the multi-wavelength network. The most important parameters dealing with performance are the tuning range and the tuning speed. The tuning range defines the wavelength range in which the filter is operational. The tuning speed decides how fast a filter can reset from one wavelength to another. Other important features include narrow bandwidth, high side-lobe suppression, simple control mechanism for a tunable optical filter, small size, and cost-effectiveness.

The next generation of high-speed communication systems will need to support the aggregate bandwidth and low

latency requirements of current and future applications such as Internet access, high-quality videoconferencing, and multimedia traffic. *Static* dense wavelength-division multiplexing (WDM) is currently becoming the leading technology in point-to-point transmission links. In the next stage, *dynamic* WDM technology is expected to take over and support full functionality on the system and network levels. Circuit-switching, moderate-speed functionalities such as optical filtering, optical add-drop multiplexing, wavelength conversion, and optical cross connects seem to be the main goals in the near term. In the long term, packet and cell switching required in Internet Protocol (IP) and asynchronous transfer-mode (ATM) applications will require ultra-high-speed manipulations. Since in WDM systems each channel is related to a different wavelength, channel manipulations and particularly channel selection require optical wavelength selection (i.e., optical filtering). Important filter parameters include insertion loss, bandwidth, side-lobe suppression, dynamic range, tuning speed, control mechanism, size, and mass-production possibility. The various filter technologies are being designed in a way to best fit the above parameters in WDM applications. For example, a WDM International Telecommunication Union (ITU) standard grid for channel spacing of 0.8 nm (100 GHz) has already been defined, and in some systems 0.4 nm (50 GHz) of channel spacing is being implemented. In addition, a requirement for –20-dB or –30-dB channel isolation should be met by each filter technology, and the tuning range is required to cover the entire 40-nm Erbium-doped fiber amplifier (EDFA) spectral range. Generally, tunable optical filters can be divided application-wise into two main categories:

- slow-speed tunable, with tuning times up to a few mil-

liseconds, relevant for circuit-switched networks,

- high-speed tunable, in the microsecond and nanosecond range, relevant for packet- and cell-switching networks.

The first category is mostly based on temperature or mechanical effects and is in the advanced development stage. Many techniques and devices are already commercially available. On the other hand, most devices in the high-speed category are still in different phases of the research stage. Among this category, microsecond devices have already made significant progress (and some have recently become commercial), while most nanosecond devices are still in the preliminary research stage for cell-switching networks. Cell switching closely resembles packet switching, but it breaks a data stream into packets, which are then placed on lines that are shared by several streams. The major difference is that cells have a fixed size while packets can have different sizes. In principle, this makes it possible to offer bounded delay guarantees.

Surface micromachining is one of the promising technologies to fabricate optoelectronic and light-wave propagation devices. Using the micromachining technique, a new approach to fabrication of the Fabry–Perot tunable filters with a gap between two distributed Bragg reflectors (DBR) is possible. Integrating a movable cantilever^{6–8} or a moving membrane^{9,10} with the DBR pairs results in surface micromachined wavelength-tunable filters. The tuning concepts can be based on electrostatic, acoustic, thermal actuation, and electromagnetic actuation^{11,12} of the moving mirror membrane. Micromachined TOFs have a wide tuning range, low insertion loss, and narrow bandwidth.

Modeling and simulation play important roles in the design of micro-electromechanical systems. In this paper, we investigate various designs of the micro-mirror for tunable optical filters. The key to accomplish a tunable MEM filter is controlling the movement of the top mirror. By a proper adjustment in the potential difference between the top and bottom DBR mirrors with the possible necessity to use a control feedback signal, the gap between the two mirrors can be precisely adjusted. This shortens the length of the Fabry–Perot cavity, and a blue shift in the resonant wavelength is observed. Based on combined mechanical and optical simulation results, tuning characteristics of the micro-mechanically tunable filter have been investigated.

2 MEM Mirror Design Considerations

A simple representation of the MEM filter consisting of an air gap that separates the top gold-plated mirror and the bottom DBR mirror is shown in Fig. 1.

A membrane with a post supports the top movable mirror. Voltage is applied between the top and bottom mirrors, which acts as the tuning mechanism for the Fabry–Perot filter. The resonant wavelength of the Fabry–Perot filter is proportional to the cavity length. Equation (1) gives the resonant wavelength, λ_m :

$$\lambda_m = \frac{2nL}{m}, \quad (1)$$

where n is the refractive index of the medium inside the FP cavity, λ_m is the m th corresponding wavelength, and L is

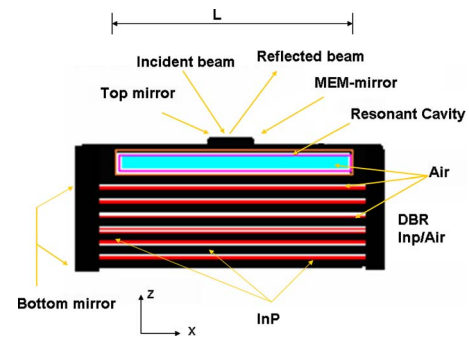


Fig. 1 MEM mirror for Fabry–Perot optical filter.

the cavity length. The wavelength of the transmitted or blocked medium can then be modulated by shifting the FP resonance, either by changing the refractive index, n , or the effective length of the cavity, L . The larger the displacement of mirror toward the bottom mirror is, the larger is the tuning range. The tuning speed is another important parameter. A slower tuning speed causes more delay between the voltage and the position of the MEM mirror. Mechanical resonant frequency as a first approximation determines the tuning speed, i.e., the higher the frequency, the faster the tuning speed. Equation (2) represents the electrostatic force per unit area generated on the membrane when voltage V is applied between the top and the bottom mirrors:^{13,14}

$$f_e = \frac{F}{A} = \frac{\epsilon_0 V^2}{2(L - \Delta L)^2}. \quad (2)$$

We have considered four mirror designs, which are shown in Fig. 2. Design 1 has crab-shaped springs connecting the central mirror to the peripheral post and has a displacement tuning range of 98 nm in the vertical direction with an actuation voltage of 35 V for mirror with dimensions $100 \mu\text{m} \times 100 \mu\text{m}$.¹³

The spring structures on the arms make Designs 2, 3, and 4 different from design 1. The material of the mirror

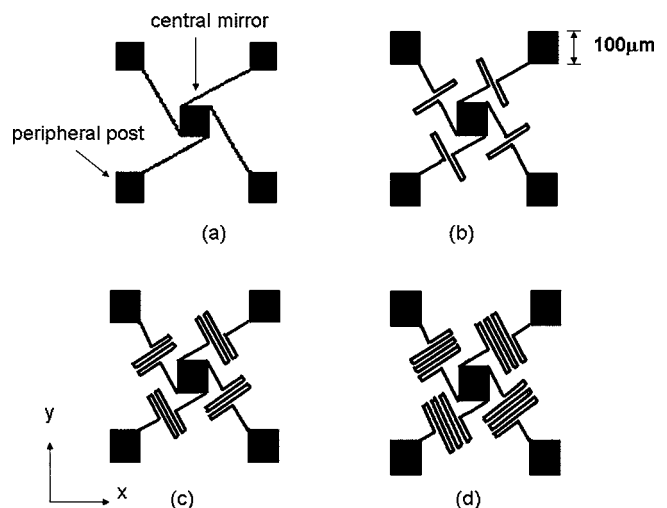


Fig. 2 Four mirror designs: (a) design 1; (b) design 2; (c) design 3; (d) design 4.

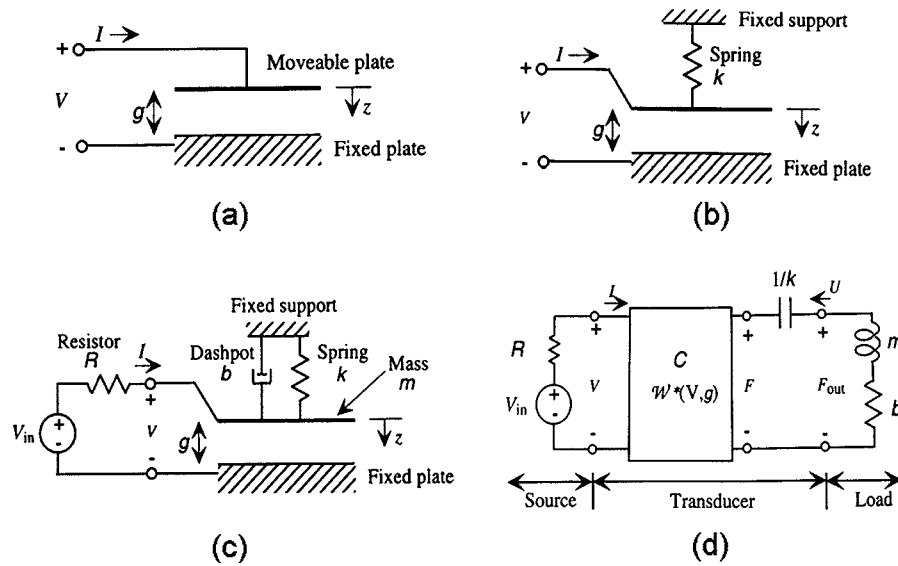


Fig. 3 Models of the micro-mirror as electrostatic actuator.

model is poly-silicon. The mirror size was designed to be $100 \times 100 \mu\text{m}$ in length and $50 \times 50 \mu\text{m}$ in width. The peripheral posts are $100 \times 100 \mu\text{m}$ at the base. The arms connecting the posts and the top mirror are $10 \mu\text{m}$ wide. The length of the arms varies with the spring structure on the arms. In order to study how the models work in operating conditions, CoventorWare™ was used to create MEMS solid models. Voltages between 0 to 2.5 V were applied to find the displacement of the top mirror toward the bottom mirror.

3 Electromechanical Simulations

To analyze MEM mirrors, we need to create some theoretical models. It starts by modeling a parallel-plate capacitor with one movable plate, as shown in Fig. 3.¹³ The parameters are listed in Table 1. Because of the opposite charges on the two plates, there is an attraction force between the plates. In fixed-plate electrical capacitors, we do not consider this force, but it is always present, whenever the capacitor is charged. When one plate is movable, the inclusion of this mechanic force becomes essential. Without some mechanical support providing an equal and opposite force on the upper plate, the two plates would move together. Therefore, it leads to the idea of two-port elements: an electrical port with voltage and current (the time derivative of charge) as variables, and a mechanical port with force and velocity (the time derivative of displacement) as variables.

Let us analyze this movable- and parallel-plate capacitor. First consider it under the condition of a fixed gap, g . The capacitance is given by Eq. (3):

$$C = \frac{\epsilon A}{g} \tag{3}$$

The stored energy, in general, for a capacitive element with effort e and displacement q is

$$W(q) = \int_0^q e(q) dq. \tag{4}$$

For the electrical capacitor in the e to V convention, e is written as V and q as Q . Since

$$Q = CV, \tag{5}$$

the expression for the stored energy becomes

$$W(Q) = \int_0^Q \frac{Q}{C} dQ = \frac{Q^2}{2C} = \frac{Q^2 g}{2\epsilon A}. \tag{6}$$

Table 1 Parameters used in the modeling of the electrostatic tuning system.

Parameter	Symbol
Area	A
Permittivity	ϵ
Initial gap	g_0
Minimum gap	g_{\min}
Mass	m
Damping	B
Spring	K
Resistance	R
Voltage	V_{in}
Capacitance	C
Stored energy	$W(v, g)$

Now consider the impact of change of the gap, g . The force between the plates set up by the charges $+Q$ and $-Q$ on opposite plates depends on the electrical field set up by the charges. The field is

$$E = \frac{Q}{\epsilon A}, \quad (7)$$

and the corresponding force is

$$F = \left(\frac{Q}{2}\right)E = \frac{Q^2}{2\epsilon A}, \quad (8)$$

where the factor 2 beneath Q is used to avoid double-counting of the charge. If the gap changes, the work that needs to be done is

$$W(g) = Fg = \frac{Q^2 g}{2\epsilon A}, \quad (9)$$

which is the same stored energy as when calculating the electrostatic stored energy $W(Q)$ at fixed g .

Therefore, the stored energy in this parallel-plate capacitor is a function of an electrical variable (charge) and a mechanical variable (displacement, or gap). We can construct a set of differentials to describe how the stored energy changes according to the change of the gap, g , or the charge, Q :

$$dW = Fdg + VdQ. \quad (10)$$

Using this formulation, we can write

$$F = \left. \frac{\partial W(Q, g)}{\partial g} \right|_Q = \frac{Q^2}{2\epsilon A} \quad (11)$$

and

$$V = \left. \frac{\partial W(Q, g)}{\partial Q} \right|_g = \frac{Qg}{\epsilon A} = \frac{Q}{C}. \quad (12)$$

Now, we can apply these ideas to the basic electrostatic actuator by adding a spring between the movable plate and a fixed support, as shown in Fig. 3(b). Assume that the rest-position gap (with zero spring force and zero capacitor charge) is g_0 . Furthermore, we want to add dynamics to the model. To do so, we include a mass to represent the mechanical inertia of the moving mirror. This is equivalent to a dashpot system to capture the mechanical damping forces that arise from the viscosity of the air, since the air must be squeezed out when the mirror moves down and drawn in when the mirror moves up. The dashpot also contains a source resistor for the voltage source that drives the tuning system, as well as a spring between the movable mirror and a fixed electrode plate. This enhanced model is shown in Fig. 3(c), while the equivalent circuit model is shown in Fig. 3(d).

It is clear from the equivalent circuit that the two-port capacitor is the essential element of the micro-mirror, with one port in the electrical domain and the other in the mechanical domain. We need to create the governing equations for the system. For the electrical domain, we have

Table 2 Actual values of parameters used in the simulation.

Parameter	Symbol	Value
Area	A	100
Permittivity	ϵ	1
Initial gap	g_0	1
Minimum gap	g_{\min}	0.01
Mass	m	1
Damping	b	0.5
Spring	k	1
Resistance	R	0.001

$$Q = I = \frac{1}{R}(V_{\text{in}} - V) = \frac{1}{R}\left(V_{\text{in}} - \frac{Qg}{\epsilon A}\right). \quad (13)$$

For the mechanical domain, using the force from Eq. (11), we obtain

$$\frac{Q^2}{2\epsilon A} + bg + mg + k(g - g_0) = 0. \quad (14)$$

Therefore, the state equations are

$$\dot{Q} = \frac{1}{R}\left(V_{\text{in}} - \frac{Qg}{\epsilon A}\right),$$

$$\dot{g} = v,$$

$$\dot{v} = -\frac{1}{m}\left(\frac{Q^2}{2\epsilon A} + k(g - g_0) + bg\right). \quad (15)$$

To examine the dynamic behavior of the system reflected by the solutions of these state equations, S. D. Senturia¹⁴ performed simulations in Simulink using the parameters as shown in Table 2.

There is a time lag between the applied voltage and the appearance of the charge on the plate because of the finite resistance R . The pull-in voltage is

$$V_{\text{PI}} = \sqrt{\frac{8kg_0^3}{27\epsilon A}}. \quad (16)$$

At V_{PI} , the growth of the electrostatic force becomes dominant over the linearly increasing mechanical restoring force, and the mirror quickly pulls into the bottom electrode. We note the very clear pull-in event followed by the release, once the charge decreased again to a small value.

The spring structure as shown in Fig. 4 was chosen due to its ability to provide both very low values of spring constant in a compact area as well as high cross-axis sensitivity between the vertical and lateral dimensions.^{15,16} The

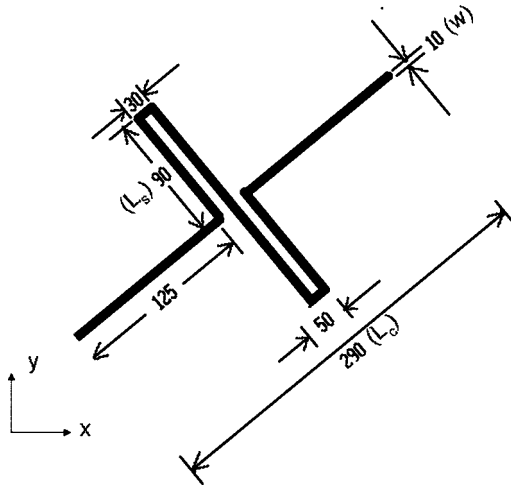


Fig. 4 Spring structure used in membrane to support mirror (all units are in μm).

number of spring meanders is varied according to the design. Eq. (17) gives the spring constant in the z -direction, k_z for one of the suspensions:^{17,18}

$$k_z = \frac{Ew \left(\frac{t}{L_c} \right)^3}{1 + \frac{L_s}{L_c} \left(\left(\frac{L_s}{L_c} \right)^2 + 12 \frac{1+\nu}{1 + \left(\frac{w}{t} \right)^2} \right)}, \quad (17)$$

where E and ν are the Young's modulus and Poisson's ratio for the metal, respectively, t is the spring thickness in the z -direction; w is the spring thickness in the xy -plane; L_s is the maximum width of the spring; and L_c is the maximum length of the spring, as indicated in Fig. 4. The total spring constant is the sum of all four suspensions attached to the structure represented by Eq. (17):

$$K_z = \frac{4k_z}{N}, \quad (18)$$

where N is the number of meanders. The spring constant decreases linearly with successive addition of meanders to the folded suspension.

4 Optical Simulations of the DBR Mirror

Optical simulations play important roles in the design and performance of the device. The design of the optical filter consists of a bottom DBR mirror and a gold-plated MEM mirror separated by an air-resonant cavity. In the previous section, electromechanical simulations were discussed. Now we will discuss the optical simulations for the optical filter. From Fig. 5, we can see that the optical filter is a vertical-cavity structure. The DBR consisting of periodic quarter-wavelength stacks of low- and high-refractive-index compound semiconductors, as shown in Fig. 5, is used in the fabrication.

For the optical filter, it is crucial to calculate the reflectivity of the DBR structure and MEM mirrors. In general, the matrix method¹⁹ may be used for the numerical calcu-

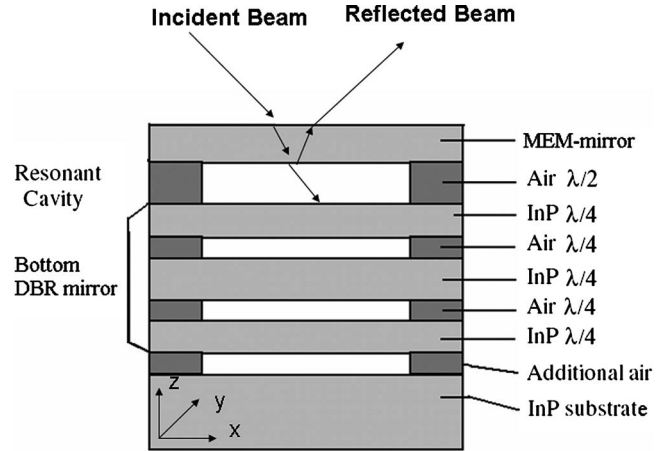


Fig. 5 Micromachined optical filter structure.

lation of the reflectivity. We have used a simple and rapid numerical technique explained for the reflectivity calculations.

The thin-film method developed by Matin et al.²⁰ and based on thin-film optics is a simple and quick numerical technique used for simulations of DBR mirror design. In this method, all the partial reflections within a layer are summed, and the process is then extended layer by layer to include the entire mirror stack.

Figure 6 shows an electromagnetic wave with electric field E of unit amplitude, polarized parallel or perpendicular to the plane of incidence, obliquely incident from layer 1 of complex refractive index n on to layer 2 of complex refractive index n . The incident beam is partially reflected and partially transmitted at the first interface. By calculating the partial reflectance and partially transmittance at each layer in the DBR structure, it can be passed on to the consecutive layer. The reflectance and transmittance of the beam calculated at the last layer of the structure give the resultant reflectance and transmittance. The reflection and transmission coefficients for each layer are given by Eqs. (19) and (20):

$$R_i = \frac{R_i + r_{i,i+1} e^{-j\delta_i}}{1 + R_{i-1} r_{i,i+1} e^{-j\delta_i}}, \quad (19)$$

$$T_i = \frac{T_{i-1} t_{i,i+1} e^{-j(\delta_i/2)}}{1 + R_{i-1} r_{i,i+1} e^{-j\delta_i}}, \quad (20)$$

where $\delta_i = (4\pi/\lambda_0) n_i d_i$. For N layers in the DBR structure, the overall reflection and transmission coefficients R_N and T_N are obtained by iterating layer by layer through layers 1 and 2.

To find R_N , an algorithm was developed in Java, based on the thin-film method.²⁰ The program implements the equation for N layers of the DBR mirror and calculates the reflective coefficient for a particular range of wavelengths. Layer thickness and reflective indices of the material for the wavelength range are used as the input parameters for obtaining the solution. For optical simulation we have used an InP/air-gap material system as the alternating pairs for the bottom mirror. InP/air-gap Bragg mirrors have a very

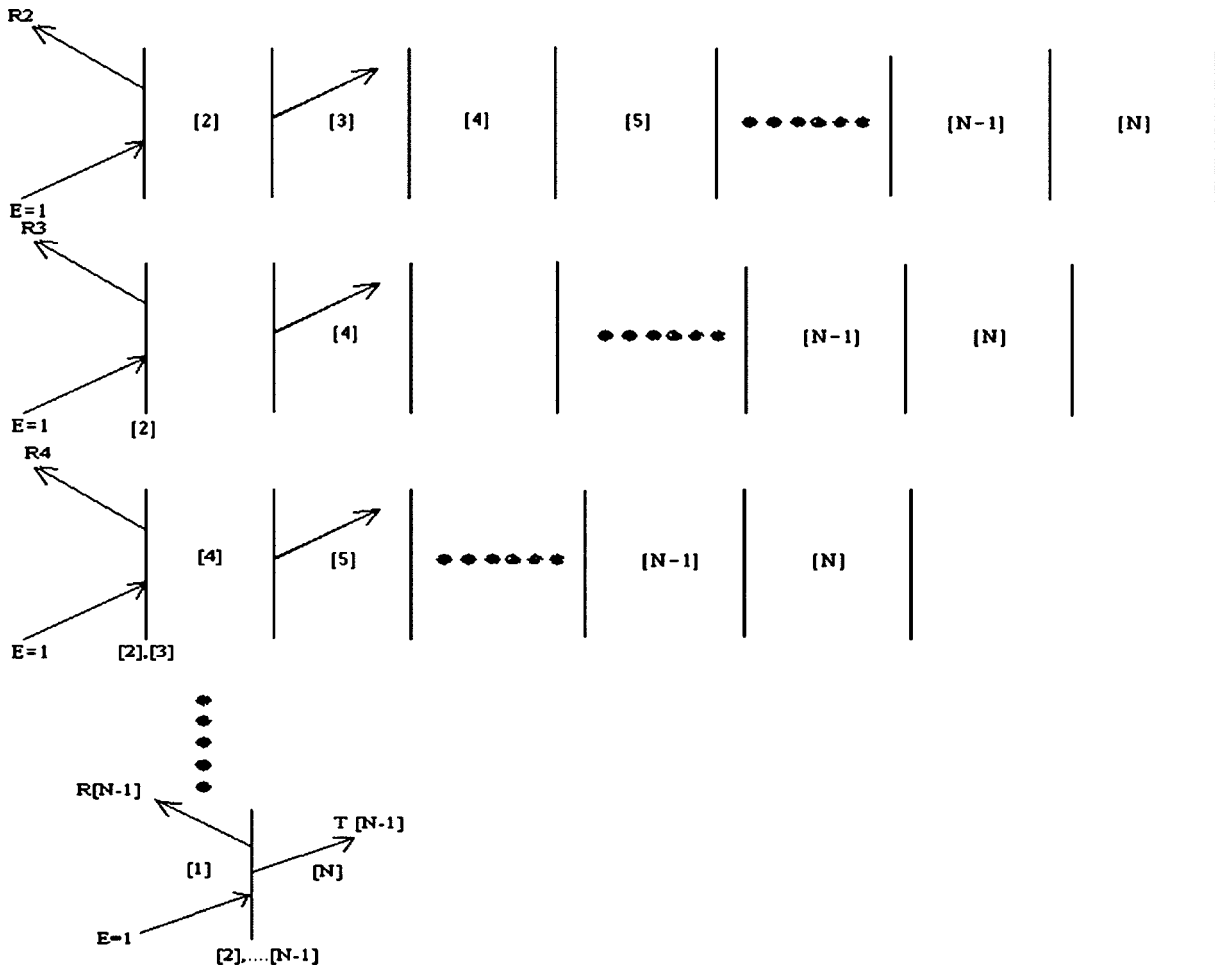


Fig. 6 Reflection and transmission coefficients of layers [2], [3], ..., [N].

high refractive-index contrast, i.e., $n_{InP}=3.167$ and $n_{air}=1$.²¹ This has an advantage of requiring many fewer layer periods for the same reflectivity. For InP material, the refractive index's dependency on wavelength is calculated using Sellmeier's formula, as follows:

$$n_s^2 = 7.194 + \frac{2.282\lambda^2}{\lambda^2 - 0.422 \times 10^6}, \quad (21)$$

where the λ are measured in nm.

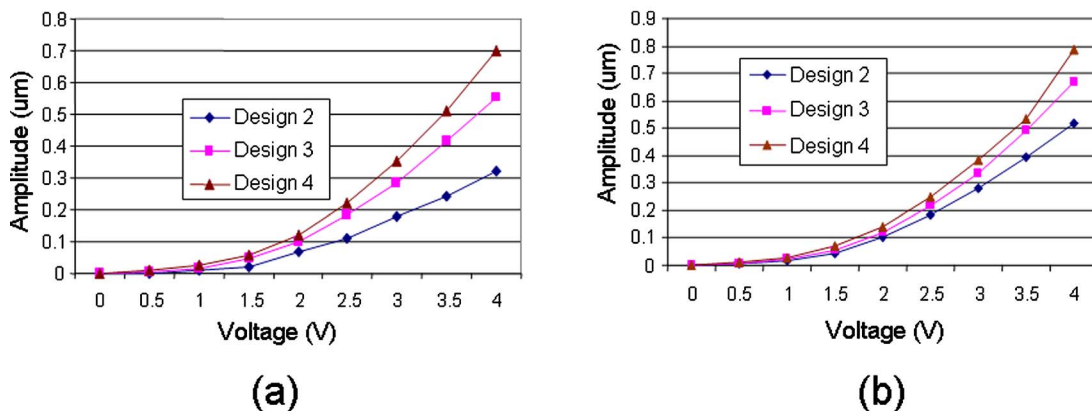


Fig. 7 Maximum amplitude (μm) vs voltage (V) for designs: 2, 3, & 4. (a) Mirror dimension $100 \times 100 \times 2 \mu\text{m}$; (b) mirror dimension $50 \times 50 \times 2 \mu\text{m}$.

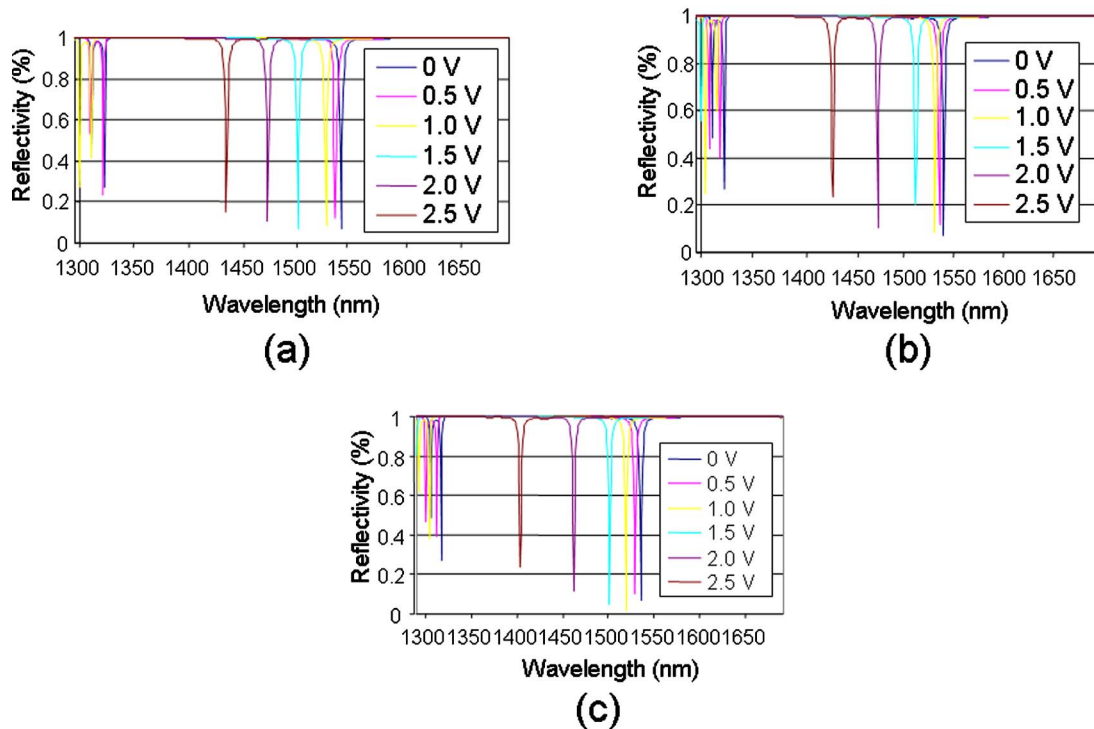


Fig. 8 Reflectivity (%) vs wavelength (nm) at different voltages with mirror dimension $100 \times 100 \mu\text{m}$. (a) Design 2 with tuning range of 106 nm; (b) design 3 with tuning range of 110 nm; and (c) design 4 with tuning range of 132 nm.

Accurate values of InP can be obtained for the 1300–1600-nm wavelength range. The Java program has been used to calculate the reflectivity of the mirror stack, including the top gold-plated MEM mirror. The output of the program gives the reflectance at respective wavelengths between 1300–1600 nm. The simulation results for electro-mechanical and optical simulations will be presented in Section 5. Also, combining both simulations, the tunability characteristics of the MEM-based optical filter will be presented.

5 Analysis and Results

Figure 7 shows the simulation results related to the maximum deflection amplitudes in designs 2–4 for two different mirror dimensions. In both cases, design 4 shows the largest amplitude of deflection, the next-largest is design 3, and, finally, design 2. This result is true for any actuation voltage. Therefore, the design of the folded suspension is of crucial importance in realizing an MEMS mirror with low actuation voltage.

Electromechanical simulations provide the displacement of the top mirror, while the optical simulation gives the filter characteristics, i.e., reflectivity for a range of wavelengths. Results from both simulations are combined to obtain the tuning behavior of the filter at 1550 nm when the top mirror is subjected to electrostatic force. Mirrors with small dimensions have a higher resonant frequency, giving a higher tuning speed.

The tuning ranges for different designs are shown in Figs. 8 and 9. In the figures it can be seen that the wavelength monotonically decreases with the applied voltage. The tuning range can be obtained from the difference be-

tween the maximum and minimum tunable wavelengths. It can also be seen that, under any voltage, the tuning range increases as the number of springs increases. For example, from Figs. 8(c) and 9, we can see that design 4 has the largest tuning range of 132 nm at 2.5 V, compared to design 3 (110 nm), design 2 (106 nm), and design 1 (98 nm). The pull-in voltage V_{PI} is given by Eq. (15).

At V_{PI} , the growth of the electrostatic force becomes dominant over the linearly increasing mechanical restoring force, and the mirror quickly pulls into the bottom electrode. Figure 8 shows that a low voltage of 2.5 V is re-

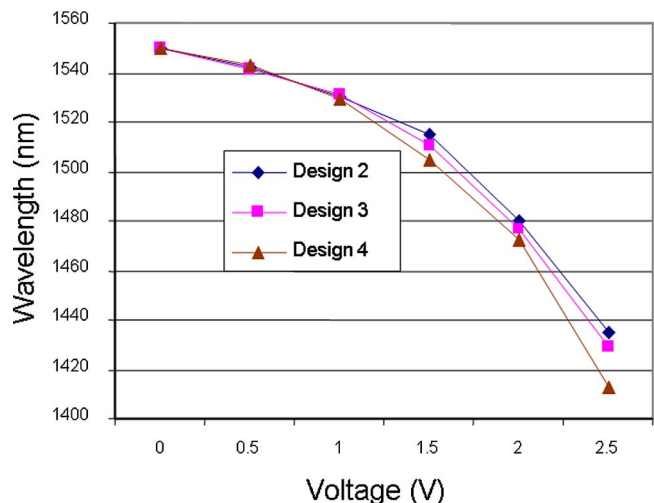


Fig. 9 Wavelength (nm) vs voltage (V) analysis for mirrors.

quired to actuate and obtain a wide tuning range in all designs. The voltage required to tune is much lower than the pull-in voltage. The average pull-in voltage of designs is 4.5 V. This reduces the probability of the top mirror's snapping down to the bottom mirror.

Conclusions

We have shown the modeling optimization of the MEM mirror for optical filters. Applying a spring structure to the membrane greatly reduces the actuation voltage and achieves a wide tuning range. Based on both electromechanical and optical simulations, the micromechanical tuning behavior has been investigated. A wide tuning range of 149 nm for an actuation voltage of 2.5 V is achieved. To the best of our knowledge, this is one of the widest possible tuning ranges reported to date for such a low actuation voltage.

References

1. S.-S. Yun and J.-H. Lee, "A micro machined in-plane tunable optical filter using the thermo-optic effect of crystalline silicon," *J. Micro-mech. Microeng.* **13**, 721–725 (2003).
2. J. Stone and L. W. Stulz, "Pigtailed high finesse tunable FP interferometer with large, medium and small FSR," *Electron. Lett.* **23**, 781–783 (1987).
3. A. Iocco, H. G. Limberger, R. P. Salathe, L. A. Everall, K. E. Chisholm, J. A. R. Williams, and I. Bennion, "Bragg grating fast tunable filter for wavelength division multiplexing," *J. Lightwave Technol.* **17**, 1217–1221 (1999).
4. D. Brooks and S. Ruschin, "Integrated electrooptic multielectrode tunable filter," *J. Lightwave Technol.* **13**, 1508–1513 (1995).
5. H. Herrmann, K. Schafer, and C. Schmidt, "Low loss tunable integrated acoustooptical wavelength filter in LiNbO₃ with strong side-lobe suppression," *IEEE Photonics Technol. Lett.* **10**, 120–122 (1998).
6. E. C. Vail, M. S. Wu, G. S. Li, L. Eng, and C. J. Chang-Hasnain, "GaAs micromachined widely tunable Fabry–Perot filters," *Electron. Lett.* **31**(3), 228–229 (1995).
7. M. S. Wu, E. C. Vail, G. S. Li, W. Yeun, and C. J. Chang-Hasnain, "Tunable micromachined vertical cavity surface emitting laser," *Electron. Lett.* **31**(19), 1671–1672 (1995).
8. M. S. Wu, E. C. Vail, G. S. Li, W. Yeun, and C. J. Chang-Hasnain, "Widely and continuously tunable micromechanical resonant cavity detector with wavelength tracking," *Electron. Lett.* **8**, 98–100 (1995).
9. M. C. Larson, B. Pezeskhi, and J. S. Harris, "Vertical coupled cavity microinterferometer on GaAs with deformable-membrane top mirror," *IEEE Photonics Technol. Lett.* **7**, 382–384 (1995).
10. M. C. Larson, A. R. Massengale, and J. S. Harris, "Continuously tunable micromachined vertical cavity surface emitting laser with 18 nm wavelength range," *Electron. Lett.* **32**, 330–332 (1995).
11. J. Sutanto, A. Papania, A. H. Berthelot, and P. J. Hesketh, "Dynamic characteristic of membrane displacements of a bidirectional microactuator with microcoil fabricated on a single wafer," *Microelectron. Eng.* **82**(1), 12–27 (2005).
12. J. S. Bintoro, A. Papania, A. H. Berthelot, and P. J. Hesketh, "Bidirectional microactuator with microcoil fabricated on a single wafer: Static characteristics of membrane displacements," *J. Micromech. Microeng.* **15**(8), 1378–1388 (2005).
13. Y. Guan and M. A. Matin, "Design and analysis of MEM-micromirrors for vertical-cavity surface-emitting lasers," *Microwave Opt. Technol. Lett.* **37**(6), 410–413 (2003).
14. S. D. Senturia, *Microsystem Design*, 4th ed., Kluwer, Norwell, MA (2002).
15. V. Gogte and M. A. Matin, "MEM-mirror design and analysis for optical tunable filters," *Proc. SPIE* **5511**, 199–206 (2004).
16. S. Pacheco, L. P. B. Katehi, and C. T.-C. Nguyen, "Design of low actuation voltage RF MEMS switch," *Proc. IEEE MTT-S* (2000).
17. E. P. Popov, *Introduction to Mechanics of Solids*, Prentice-Hall, Englewood Cliffs, NJ (1968).
18. J. E. Shigley and L. D. Mitchell, *Mechanical Engineering Design*, 4th ed., McGraw-Hill, New York (1983).
19. L. A. Coldren and S. W. Corzine, *Diode Lasers and Photonic Integrated Circuits*, Wiley, New York (1995).
20. M. A. Matin, T. M. Benson, L. R. Chen, and P. W. E. Smith, "Analysis of distributed bragg reflectors using thin-film optics," *Microwave Opt. Technol. Lett.* **21**(1), 11–15 (1998).
21. C. Prott, F. Romer, E. Ataro, J. Daleiden, S. Irmer, A. Tarraf, and H. Hillmer, "Modeling of ultrawidely tunable vertical cavity air-gap filters and VCSELs," *IEEE J. Quantum Electron.* **9**(3), 918–928 (2003).



Mohammad A. Matin earned his BS (Honors) and MS degrees in applied physics and electronics with First Class from Dhaka University, Bangladesh, and his PhD in electrical & electronics engineering from Nottingham University in England in 1993. He then joined as post-doctoral fellow (1994–1995), and then research engineer (1995–1998) at the Center for Electro-Photonics Materials and Devices, McMaster University, Hamilton, Canada. He moved to the University of Toronto, as senior research associate (1998–2000). In March 2000, he joined as assistant professor of electrical engineering in the School of Engineering and Computer Science at the University of Denver and was promoted to associate professor with tenure in the spring of 2006. He is a senior member of the IEEE and a member of SPIE, OSA, ASEE, and Sigma Xi. His research interests include optoelectronic devices and systems, micro- and nano-electromechanical systems, and digital, optical & bio-medical signal and image processing.

Biographies and photographs of other authors not available.